Macromolecules

Article

pubs.acs.org/Macromolecules

Copper(0)-Mediated Reversible-Deactivation Radical Polymerization: Kinetics Insight and Experimental Study

Yin-Ning Zhou and Zheng-Hong Luo*

Department of Chemical Engineering, School of Chemistry and Chemical Engineering, Shanghai Jiao Tong University, Shanghai 200240, P. R. China

Supporting Information

ABSTRACT: A comprehensive kinetic model based on the mechanism of supplemental activator and reducing agent atom transfer radical polymerization (SARA ATRP) was developed to better understand the kinetics of copper(0)-mediated reversible-deactivation radical polymerization [Cu(0)-mediated RDRP]. Simulation results show that diffusional limitation on termination significantly affects on polymerization. A comprehensive description of the variation trend of soluble species and reaction rates during polymerization was illustrated by simulation. The effects on kinetics of four key rate constants (i.e., k_{a0}, k_{disp}, k_{a1}, k_{comp}) involved in Cu(0)-mediated RDRP were investigated in detail, which contributed to greater insight into the differences between the SET-LRP and SARA ATRP mechanisms. Finally, Cu(0)-mediated RDRPs of methyl methacrylate (MMA) and butyl methacrylate (BMA) were conducted to study the polymerization kinetics at 25 °C. Results of simulations and experiments performed under polymerization conditions show that the Cu(0) surface area-dependent apparent value follows the relationship of $k_{p1(4)}^{app}/k_{p2(5)}^{app} \propto (S_{1(4)}/S_{2(5)})^{1/2}$ in previously published works. Addition of an initial $Cu^{II}Br_2$ deactivator can significantly improve the controllability of polymerization and reduce the deviation of M_n from theoretical values and larger M_w/M_n at the start of polymerization.

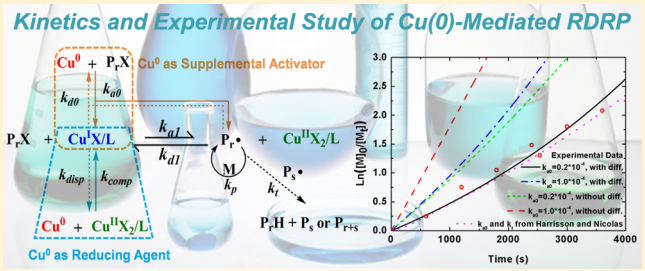

INTRODUCTION

Reversible-deactivation radical polymerization (RDRP) techniques have led to an important revolution in polymer chemistry and macromolecular reaction engineering.[1,2] Atom transfer radical polymerization (ATRP)[3,4] is a convenient RDRP method for designing and preparing functional polymer materials with well-defined structures.[5−8] The establishment of activation−deactivation equilibrium in ATRP is the core of object control, including molecular weight, polydispersity, and chain-end functionality. In an activation process, a lower oxidation state transition metal/ligand complex (usually Cu^IX/L) abstracts halogen (X) from an organic initiator (RX or P_rX) to generate a growth radical ($R^\bullet$ *or* $P_r^\bullet$). The unavoidable radical termination at low polymerization level leads to accumulation of the persistent deactivator ($Cu^{II}X_2$/L), which is known as the persistent radical effect;[9] this condition deactivates the growth chain ($R^\bullet$ *or* $P_r^\bullet$) and suppresses the irreversible termination.

Despite its technological promise, high catalyst residues (commonly Cu salt) which produces toxic products, hinder the industrialization of ATRP technique.[10−12] Many studies have been conducted to reduce the usage of catalyst in Cu-based ATRP so that environmentally harmful products will be reduced, and large scale separation and purification will be avoided.[12,13] Matyjaszewski et al. initiated the relevant studies by reducing the excess deactivator back to activator using different reducing sources,[13−16] such as initiators for continuous activator regeneration (ICAR) ATRP,[13] activators regenerated by electron transfer (ARGET) ATRP,[14] electrochemically mediated ATRP (*e*ATRP),[15] and photochemically mediated ATRP.[16] In recent years, RDRP using Cu(0) powder or wire received great attention because of its extremely low dissolved copper concentration and reusability of the Cu(0) wire.[17−23] However, two mechanisms for Cu(0)-mediated RDRP are proposed based on the different roles of the Cu species.[24−37] Percec et al. pointed out that Cu(0)/L [e.g., active ligand (L), hexamethylated tris(2-aminoethyl)amine (Me_6TREN)] reacts with RX or P_rX to form $R^\bullet$ *or* $P_r^\bullet$ and Cu^IX/L; the latter being instantaneously disproportionated to $Cu^{II}X_2$/L and Cu(0) in polar surroundings [e.g., dimethyl sulfoxide (DMSO)]; this mechanism is named single electron transfer-living radical polymerization (SET-LRP).[24−28] Matyjaszewski et al. affirmed that Cu(0) acts both as a supplemental activator and a reducing agent (SARA) in RDRP, where Cu^IX/L is the major activator.[28−34] Harrisson et al. gave insights into the initiation period of Cu(0)-mediated RDRP in nonpolar and polar solvents, which show that above two mechanisms are not totally incompatible.[35,36] More recently, Harrisson and Nicolas[37] derived the activation and termination rate constants

Received: June 28, 2014
Revised: August 19, 2014
Published: September 3, 2014

dx.doi.org/10.1021/ma501335j | Macromolecules 2014, 47, 6218−6229

with chain length dependence from a set of experimental data reported by Percec et al.[27] for the first time.

Kinetic modeling as a supplement to experiments is a very powerful tool that helps in better understanding and optimizing ATRP processes.[38−55] Zhu et al. studied the effect of diffusion limitation and programmed synthesis of gradient copolymer through kinetic modeling of conventional ATRP based on the method of moments.[38−40] Matyjaszewski et al., Reyniers et al., and Soares et al. investigated the kinetics of various ATRP systems using the method of moments, Predici software, and dynamic Monte Carlo simulation, including conventional ATRP, reverse ATRP, simultaneous reverse and normal initiation (SR&NI) ATRP, and ICAR ATRP.[41−46] Recently, Luo et al. performed the triplet synthesis methodology-molecular structure-materials properties multiscale study on the basis of model design.[47−50] With the development of the ATRP technique, kinetic modeling was implemented in ARGET ATRP, which is a modified ATRP technique with really low copper levels (<50 ppm).[51,52] In addition, Monteiro et al.[53] and Haehnel et al.[54] investigated the kinetics of SET-LRP based on kinetic modeling. Matyjaszewski et al. presented the comparison and assessment of SET-LRP and SARA ATRP mechanisms through holistic and detailed experiments, including kinetic study.[31−34,55]

In this study, a novel and comprehensive kinetic model was developed based on the mechanism of SARA ATRP, which was validated by experimental study under classical conditions of methyl acrylate (MA) polymerization.[55] Additional experiments were used to assess and guide the synthesis of methacrylate polymerization systems using methyl methacrylate (MMA) and butyl methacrylate (BMA). Simulation was carried out using the method of moments, which is suitable for the description of polymerization characteristics including diffusional limitation effect on termination. We aimed to shed light on Cu(0)-mediated RDRP through the combination of model development and experiments, to acquire an improved understanding of the underlying mechanism, and to optimize product quality by model guidance.

Kinetic Model and Computational Method. Table 1 shows the set of kinetic model reactions used in all of the simulations conducted based on the SARA ATRP mechanism. The orange rectangular and blue trapezoid dashed frames presented in Scheme 1 shows the different roles of Cu(0) in SARA ATRP. The various lines or dashed arrows represent different reaction extent. Besides the typical ATRP reactions, such as initiation, propagation, activation deactivation equilibrium, and termination, vital copper-based comproportionation−disproportionation equilibrium reactions were considered. However, chain transfer to monomer, solvent, and polymer that led to branch formation were neglected because of their limited contribution in radical polymerizations of acrylates at low temperature conditions.[52,55,56]

The molar balance equations (i.e., kinetic equations) involving the propagating radical chain ($P_r^\bullet$), dormant chain (P_rX), and dead chain (P_r) species with the length of chain (r) are summarized in Table 2. A new parameter $\varepsilon(=S/V)$ in cm^{-1} was defined because of the heterogeneous solution polymerization with copper wire; the objective of adding this parameter was to unify the units used in mass balances equations. The copper surface area dependence of the rate constants, k_{a0}, k_{d0}, k_{comp}, and k_{disp}, are expressed in $cm{\cdot}s^{-1}$, while the other rate coefficients are in $L{\cdot}mol^{-1}{\cdot}s^{-1}$ as shown in Table 3.

Table 1. Proposed Reactions of SARA ATRP

type of reaction	scheme
initiation	$P_0X + Cu^0 + L \underset{k_{d0}}{\overset{k_{a0}}{\rightleftharpoons}} P_0^\bullet + Cu^{I}X/L$
	$P_0X + Cu^{I}X/L \underset{k_{d1}}{\overset{k_{a1}}{\rightleftharpoons}} P_0^\bullet + Cu^{II}X_2/L$
	$P_0^\bullet + M \xrightarrow{k_{in}} P_1^\bullet$
comp.−disp. equilibrium	$Cu^0 + Cu^{II}X_2/L + L \underset{k_{disp}}{\overset{k_{comp}}{\rightleftharpoons}} 2Cu^{I}X/L$
propagation	$P_r^\bullet + M \xrightarrow{k_p} P_{r+1}^\bullet$
ATRP equilibrium	$P_rX + Cu^0 + L \underset{k_{d0}}{\overset{k_{a0}}{\rightleftharpoons}} P_r^\bullet + Cu^{I}X/L$
	$P_rX + Cu^{I}X/L \underset{k_{d1}}{\overset{k_{a1}}{\rightleftharpoons}} P_r^\bullet + Cu^{II}X_2/L$
termination	$P_0^\bullet + P_0^\bullet \xrightarrow{k_{t0}} P_0P_0$
	$P_r^\bullet + P_0^\bullet \xrightarrow{k_{tR}} P_rP_0$
	$P_r^\bullet + P_s^\bullet \xrightarrow{k_{td} \text{ or } k_{tc}} P_rH + P_s^{2-} \text{ or } P_{r+s}$

Scheme 1. Proposed Cu(0)-Mediated RDRP Mechanism

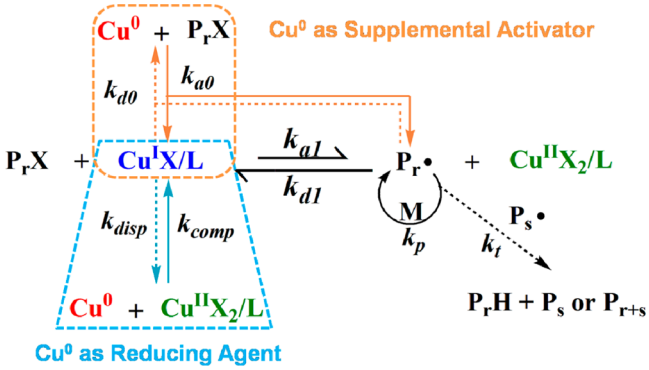

The method of moments is easy to apply in the kinetic modeling of radical polymerization processes.[38−40,42,47−51] On the basis of Zhu's work,[38] the definitions of moments for the above three chain species and a set of moment equations including all of the components are shown in Tables S1 and S2 (see Supporting Information), respectively. Accordingly, the different polymerization behaviors, namely, the number-average chain length (r_n), weight-average molecular chain length (r_w), molecular weight distribution (M_w/M_n), and chain-end functionality (F_t) can be described as follows:

$$r_n = \frac{\sum(\lambda^1 + \mu^1 + \tau^1)}{\sum(\lambda^0 + \mu^0 + \tau^0)} \quad (1)$$

$$r_w = \frac{\sum(\lambda^2 + \mu^2 + \tau^2)}{\sum(\lambda^1 + \mu^1 + \tau^1)} \quad (2)$$

$$M_w/M_n = \frac{r_w}{r_n} \quad (3)$$

$$F_t = (1 - N_{dead}) = \left(1 - \frac{\tau^0}{\sum(\lambda^0 + \mu^0 + \tau^0)}\right) \quad (4)$$

dx.doi.org/10.1021/ma501335j | Macromolecules 2014, 47, 6218−6229

Table 2. Kinetic Equations for Each Type of Chain Species in Heterogeneous Solution Polymerization

type of chains	mass balance equations[a]
propagating radical	$\frac{d[P_r^\bullet]}{dt} = k_p[P_{r-1}\cdot][M] - k_p[P_r\cdot][M] + \varepsilon k_{a0}[P_rX] - \varepsilon k_{d0}[P_r\cdot][Cu^IX]/[L] + k_{a1}[P_rX][Cu^IX] - k_{d1}[P_r\cdot][Cu^{II}X_2] - k_{tR}[P_r\cdot][P_0\cdot] - \sum_{s=1}^{\infty}(k_{tc}+k_{td})[P_r\cdot][P_s\cdot]$
dormant	$\frac{d[P_rX]}{dt} = \varepsilon k_{d0}[P_r\cdot][Cu^IX]/[L] - \varepsilon k_{a0}[P_rX] + k_{d1}[P_r\cdot][Cu^{II}X_2] - k_{a1}[P_rX][Cu^IX]$
dead	$\frac{d[P_r]}{dt} = k_{tR}[P_r\cdot][P_0\cdot] + \sum_{s=1}^{\infty} k_{td}[P_r\cdot][P_s\cdot] + \frac{1}{2}\sum_{s=1}^{r} k_{tc}[P_s\cdot][P_{r-s}\cdot]$

[a]The unit of $\varepsilon = S/V$ is in cm^{-1}, units of k_{a0}, k_{d0}, k_{comp}, and k_{disp} are in $cm\cdot s^{-1}$, the other rate constants are in $L\cdot mol^{-1}\cdot s^{-1}$

Table 3. Material Properties and Kinetic Constants for Simulation

Material Properties for MA[39,57]			
ρ_m = 0.95 g·cm^{-3}	ρ_p = 1.22 g·cm^{-3}	T_{gm} = 185 K	T_{gp} = 280 K
α_m = 0.001 K^{-1}	α_p = 0.00048 K^{-1}		
Material Properties for MMA[39,57]			
ρ_m = 0.94 g·cm^{-3}	ρ_p = 1.20 g·cm^{-3}	T_{gm} = 167 K	T_{gp} = 378 K
α_m = 0.001 K^{-1}	α_p = 0.00048 K^{-1}		
Material Properties for BMA[57−59]			
ρ_m = 0.89 g·cm^{-3}	ρ_p = 1.07 g·cm^{-3}	T_{gm} = 138 K	T_{gp} = 293 K
α_m = 0.001 K^{-1}	α_p = 0.00066 K^{-1}		
Material Properties for DMSO[57]			
ρ_s = 1.10 g·cm^{-3}	T_{gs} = 190 K	α_s = 0.00088 K^{-1}	
Kinetic Constants for MA, MMA, and BMA[37,47,55,60−62]			
k_{in} (L·mol^{-1}·s^{-1})	5.80 × 10^5	6.44 × 10^3	7.37 × 10^3
k_p (L·mol^{-1}·s^{-1})	1.56 × 10^4	3.22 × 10^2	3.68 × 10^2
k_{a0} (cm·s^{-1})	0.20 × 10^{-4a}	0.40 × 10^{-4b}	0.38 × 10^{-4b}
k_{d0} (cm·s^{-1})^c	0.24 × 10^{-1}	0.13 × 10^{-1}	0.15 × 10^{-1}
k_{a1} (L·mol^{-1}·s^{-1})	2.0 × 10^2	4.0 × 10^{2b}	3.8 × 10^{2b}
k_{d1} (L·mol^{-1}·s^{-1})	2.7 × 10^8	1.5 × 10^{8b}	1.7 × 10^{8b}
k_{disp} (cm·s^{-1})	3.1 × 10^{-6}	3.1 × 10^{-6}	3.1 × 10^{-6}
k_{comp} (cm·s^{-1})	3.5 × 10^{-3}	3.5 × 10^{-3}	3.5 × 10^{-3}
k_{t0}^0 (L·mol^{-1}·s^{-1})	2.0 × 10^9	2.0 × 10^9	2.0 × 10^9
k_{tR}^0 (L·mol^{-1}·s^{-1})	1.0 × 10^8	1.0 × 10^8	1.0 × 10^8
k_{tc}^0 (L·mol^{-1}·s^{-1})	0.90 × 10^8	0.98 × 10^7	1.69 × 10^6
k_{td}^0 (L·mol^{-1}·s^{-1})	0.10 × 10^8	4.67 × 10^7	0.19 × 10^6
B_t(dimensionless)^b	0.275	0.265	0.245

[a]From ref 37.. [b]This work. [c]$k_{d0} = (k_{a0}k_{d1}k_{disp}/k_{a1}k_{comp})$ from ref 55.

The chain length dependence of termination reactions was considered in this study using free volume theory. The termination rate constant is described as[39]

$$k_t = k_t^0\left(\frac{r_n}{r_w}\right)^{x/2}\exp\left[-B_t\left(\frac{1}{v_f}-\frac{1}{v_{f0}}\right)\right] \quad (5)$$

where B_t is an adjustable parameter and v_f denotes the fractional free volume of the reaction mixture and is calculated by

$$v_f = \sum_{i=1}^{\text{no. of components}}[0.025 + \alpha_i(T - T_{g_i})]\frac{V_i}{V} \quad (6)$$

EXPERIMENTAL SECTION

Materials. Butyl methacrylate (BMA, 99%, Sinopharm Chemical Reagent Co. (SCRC)), methyl methacrylate (MMA, 99%, SCRC) was rinsed with an aqueous NaOH solution (5 wt %) to remove inhibitor, dried with $MgSO_4$ overnight and distilled before use. Methyl 2-bromopropionate (MBrP, 97%, Adamas), hexamethylated tris(2-aminoethyl)amine (Me_6TREN, 99%, Alfa Aesar), $Cu^{II}Br_2$ (99%, Acros) and dimethyl sulfoxide (DMSO, 99.9%, Alfa Aesar) were used as received. Copper (wire, diameter 1.0 mm, 99.9%, Alfa Aesar) was typically washed with methanol/HCl first and then with methanol before use.[31]

General Procedures for Polymerization of MMA and BMA. In a typical experiment, a magnetic stirrer winded by Cu(0) wire (diameter = 1.0 mm) was first placed in a Schlenk flask, then degassed and full filled with nitrogen for three times. Subsequently, the deoxygenated DMSO and monomer (MMA/BMA) previously bubbled by nitrogen for 60 min were added to the Schlenk flask, followed by Me_6TREN and MBrP. The Schlenk flask with reaction mixture was placed in 25 °C oil bath to start polymerization and expose to air after predetermined time. The solution was diluted with THF, and filtered to remove the Cu salts by passing through a basic

dx.doi.org/10.1021/ma501335j | Macromolecules 2014, 47, 6218−6229

alumina column and precipitated in methanol (for PMMA) or methanol/HCl mixture (for PBMA). The obtained polymer was rinsed with precipitant for several times and dried to constant weight under vacuum at 40 °C. At time intervals, samples were taken by syringe for kinetic analysis. Monomer conversion is measured by gravimetry and used for the calculation of Mn. The detailed polymerization conditions are list in Table 4.

Table 4. Cu(0)-Mediated RDRP of MMA/BMA in 2.5 mL DMSO at 25 °C

entry	monomer	$[M]_0/[MBrP]_0/[Me_6TREN]/[Cu^{II}Br_2]$	Cu(0) wire	$\varepsilon(S/V)$
1	MMA (5 mL, 47.14 mmol)	200/1/0.1/0	4 cm (1.27 cm^2)	0.169
2	MMA (5 mL, 47.14 mmol)	200/1/0.1/0	2 cm (0.644 cm^2)	0.086
3	MMA (5 mL, 47.14 mmol)	200/1/0.1/0.01	4 cm (1.27 cm^2)	0.169
4	BMA (5 mL, 31.69 mmol)	200/1/0.1/0	4 cm (1.27 cm^2)	0.169
5	BMA (5 mL, 31.69 mmol)	200/1/0.1/0	2 cm (0.644 cm^2)	0.086
6	BMA (5 mL, 31.69 mmol)	200/1/0.1/0.01	4 cm (1.27 cm^2)	0.169

Characterization. Monomer conversion was monitored by proton nuclear magnetic resonance (^{1}H NMR) spectroscopy (Bruker AV400 MHz) in $CDCl_3$. Molecular weights and molecular weight distributions (M_w/M_n) of the polymer using gel permeation chromatograph (GPC, Tosoh Corporation) equipped with two HLC-8320 columns (TSK gel Super AWM-H, pore size: 9 μm; 6 × 150 mm, Tosoh Corporation) and a double-path, double-flow a refractive index detector (Bryce) at 30 °C. The elution phase was DMF (0.01 mol/L LiBr, elution rate: 0.6 mL/min), and a series of poly methyl methacrylate (PMMA) were used as the calibration standard.

RESULTS AND DISCUSSION

Model Validation. The developed model for Cu(0)-mediated RDRP was validated by experimental data as reported in a previous study.[55] The present simulation was carried out under the same experimental conditions, namely, use of Cu(0) wire with l = 4 cm and d = 1 mm, $[MA]_0$:$[MBrP]_0$:$[Me_6TREN]_0$ = 200:1:0.1, V = 4.5 mL, MA/DMSO = 2/1(v/v), and at 25 °C. All of the material properties and kinetic constants (except k_{a0} and k_{d0}) were directly obtained from the same study,[55] in which the kinetic parameters were derived by experiments (Table 3). However, the simulation result in Figure 1A (red dashed line) shows that the polymerization rate ($R_{SARA\ ATRP}$) is faster than that in the practical experimental data (red circle). From the polymerization rate obtained from eq 7, it can be deduced that an increase in the radical concentration ($P^\bullet$) is the main cause of the faster polymerization rate when using conventional free radical propagation rate coefficient for simulation. According to the proposed reaction mechanism in Table 1 and the reasons (overestimated k_{a0} or underestimated k_t^0) outlined by Matyjaszewski et al.,[55] the chain length dependency of termination reactions were considered in the current study. Simulation was performed by reducing the Cu(0) activation rate constant (k_{a0} = 0.2 × 10^{-4} cm·s^{-1}) to one-fifth of the original value of k_{a0}(1.0 × 10^{-4} cm·s^{-1}) in the absence of diffusional limitation (green short-dashed line in Figure 1A), which enabled the polymerization rate to slow down, and the results to be close to the experimental data. This reduction of k_{a0} is according to the kinetic parameter reported in recent publication.[37] The blue dashed-dot line in Figure 1A shows that diffusional limitation on temonation had a

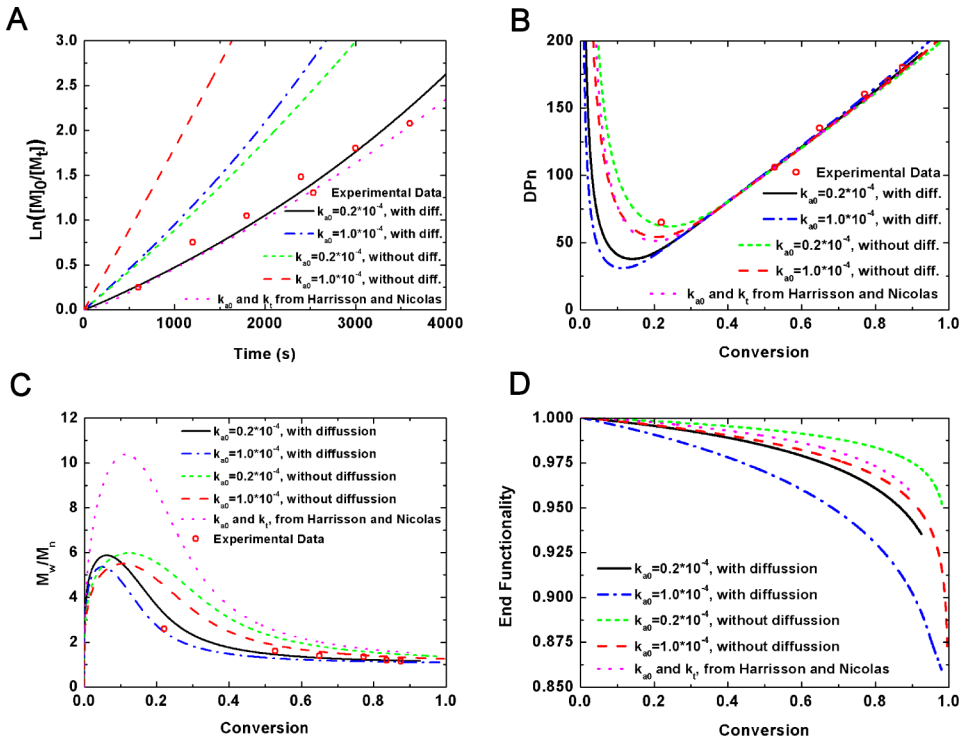

Figure 1. Model validation through experimental data for Cu(0)-mediated RDRP of MA from ref 55: (A) semilogarithmic kinetic plot; (B) evolution of DPn with conversion; (C) evolution of M_w/M_n with conversion; (D) evolution of end functionality with conversion. (The chain length dependent k_{a0} and k_t from Harrisson and Nicolas are reported in ref 37.)

dx.doi.org/10.1021/ma501335j | Macromolecules 2014, 47, 6218−6229

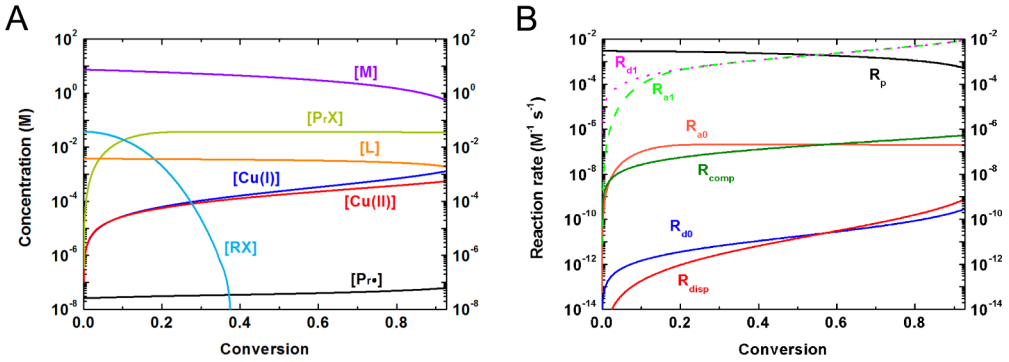

Figure 2. Evolutions of reactant concentrations (A) and reaction rates (B) during Cu(0)-mediated RDRP of MA.

pronounced effect on the polymerization kinetics using the original value of k_{a0}. Deviation from experimental data was observed. Subsequently, simulation was conducted under conditions of activation rate constant reduction and presence of diffusional limitation, the results shown in Figure 1A (black line) match the experimental data well. In addition, we also simulated the polymerization using the chain length dependent activation and termination rate constants ($k_{a0} = 1.25 \times 10^{-4}$ $DP_n^{-0.51}$ cm·s^{-1} and $k_t = 3.10 \times 10^9$ $DP_n^{-0.49}$ L·mol^{-1}·s^{-1}) derived by Harrisson et al.,[37] the results shown in the magenta dotted line also meet well with kinetics data.

In general, a downward curvature was obtained for the kinetic plot in the absence of diffusional limitation at high polymerization degree, while an upward curvature was obtained in the presence of diffusional limitation on termination, which eventually led to a linear plot like the one in living radical polymerization.[9] The linear kinetic plot indicates the nearly constant concentration of radicals in this system during polymerization [see eq 9].

$$R_{SARA\ ATRP} = -\frac{d[M]}{dt} = k_p[P^\bullet][M] \tag{7}$$

SARA ATRP differs from conventional ATRP because of the reversible activation process by Cu(0) (Scheme 1), which combines with the reversible activation process by Cu^IX/L influencing the polymerization rate, molecular weight and its distribution. Radical concentration can be calculated by derivation from the reaction rate equations of activation and deactivation by Cu(0) and Cu^IX/L based on fast equilibrium approximation.[32,63]

$$[P^\bullet] = \frac{k_{a0}[PX][L]}{k_{d0}[Cu^IX/L]} + \frac{k_{a1}[PX][Cu^IX/L]}{k_{d1}[Cu^{II}X_2/L]} \tag{8}$$

Integrating eq 7 into the initial monomer concentration at $t = 0$ ($[M]_0$) yields eq 9:

$$\ln\left(\frac{[M]_0}{[M]_t}\right) = k_p[P^\bullet]t \tag{9}$$

Substituting eq 8 into eq 9 yields eq 10:

$$\ln\left(\frac{[M]_0}{[M]_t}\right) = k_p\left(\frac{k_{a0}[PX][L]}{k_{d0}[Cu^IX/L]} + \frac{k_{a1}[PX][Cu^IX/L]}{k_{d1}[Cu^{II}X_2/L]}\right)t = k_p^{app}t \tag{10}$$

In parts B and C of Figure 1, a linear relation exists between the degree of polymerization (DP_n) and conversion, and M_w/M_n experiences an increase and rapid leveling off (<1.5) after the establishment of the ATRP equilibrium, as observed by experimental and modeling results in other groups.[53−55] The activation rate constant and diffusional limitation have different effects on the time required to attain ATRP equilibrium (i.e., the reduction of k_{a0} extends the equilibrium time and diffusional limitation shortens the time). However, both characteristics demonstrate the controllability of polymerization in all cases. Long polymer chains formation and high polydipersity result from the slow generation of $Cu^{II}X_2/L$ deactivator, which is insufficient in suppressing the irreversible termination and controlling the reaction based on persistent radical effect, especially under the condition with higher termination rate (magenta dots line). Figure 1D shows that evolutions of the end functionality decreased gradually but maintained its considerable "livingness" because of the occurrence of irreversible termination in all cases, which are only minimized in all of the RDRP techniques. However, one can find that high end functionality can obtained by lower k_{a0}, which is caused by slowing down the generation of $Cu^{II}X_2/L$.[37] As a whole, simulation results in Figure 1 show good agreement with experimental data when constant activation rate parameter and diffusional limitation are both taken into account, which demonstrate the reliability of our developed model. Succeeding studies were carried out on the basis of the present model.

Concentration of Reactants and Rate of Reactions for RDRP with Cu(0). Complete description of the variation trend concerning soluble species and the rates of reactions under the same conditions [Cu(0) wire with $l = 4$ cm, $d = 1$ mm, $[MA]_0$:$[MBrP]_0$:$[Me_6TREN]_0 = 200:1:0.1$, $V = 4.5$ mL, MA/DMSO = 2/1 (v/v), and at 25 °C] is shown in Figure 2. The equations for calculating reaction rates are listed in Supporting Information.

Starting with the activation of initiator by Cu(0) in the presence of the ligand (Table 1), major activator Cu^IX/L and radical were generated as time progressed in Figure 2A. Subsequently, Cu^IX/L activated the RX to form $Cu^{II}X_2/L$ and growth species ($P_r^\bullet$). Consequently, the amount of the initiator decreased significantly as the persistent radical ($Cu^{II}X_2/L$) accumulated and the radical reacted with the monomer to propagate the growth species. Accompany with the buildup of $Cu^{II}X_2/L$ and consumption of monomer, the rates of comproportionation between Cu(0) and $Cu^{II}X_2/L$ (R_{comp}) and propagation of $P_r^\bullet$ with monomer (R_p) should increases and slows down (Figure 2B). Thus, the rates of disproportionation of Cu^IX/L (R_{disp}) and deactivation of $P_r^\bullet$ by Cu^IX/L (R_{d0}) increase accordingly due to the higher $[Cu^IX/L]$. The vital process of copper-based comproportionation-disproportio-

dx.doi.org/10.1021/ma501335j | Macromolecules 2014, 47, 6218−6229

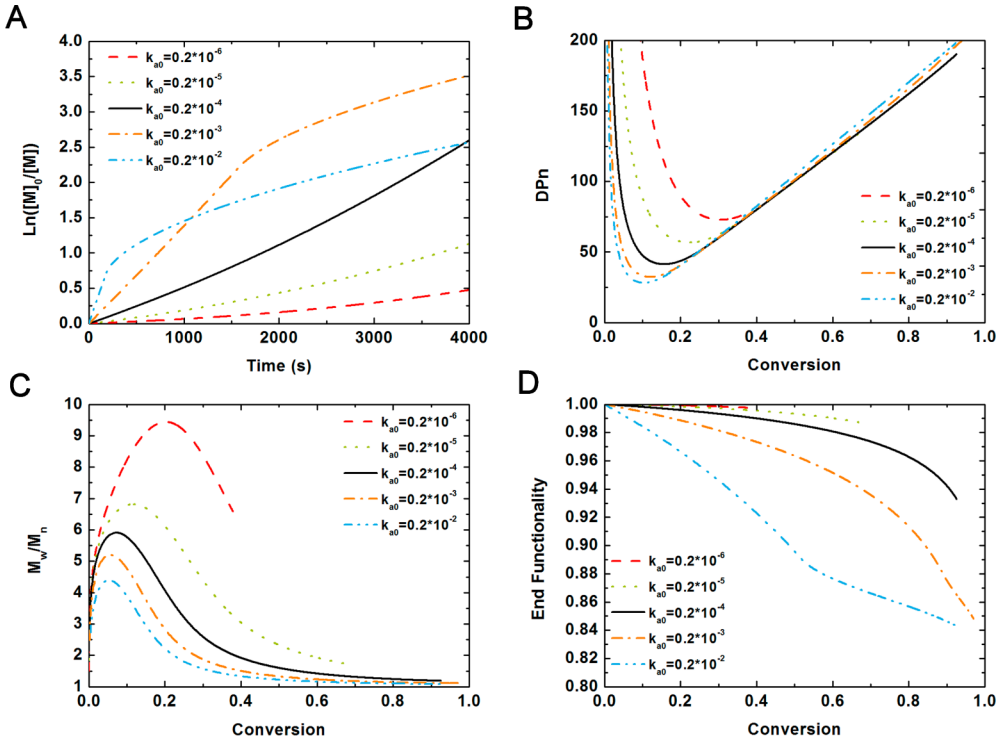

Figure 3. Effect of activation by Cu(0) (k_{a0}) on kinetics of Cu(0)-mediated RDRP of MA from ref 55: (A) semilogarithmic kinetic plot; (B) evolution of DPn with conversion; (C) evolution of M_w/M_n with conversion; (D) evolution of end functionality with conversion.

nation equilibrium would be established only after all of the initiator are consumed;[32] here, Cu(0) acts as the reductant. Concentration of the dormant species (P_rX) reached steady state at a constant value after the transition period, which is consistent with the evolution of DPn and M_w/M_n in Figure 1B,C, indicating that the activation deactivation equilibrium was attained. On other hand, as shown in Figure 2B, the evolution of R_{a1} (P_rX activation by Cu^IX/L), and R_{d1} (deactivation of $P_r^\bullet$ by $Cu^{II}X_2/L$) are overlapped after short time, which indicates that the equilibrium of ATRP is established and maintained with the progressing of polymerization; and thus the rate of P_rX activation by Cu(0) (R_{a0}) also keep uniform. In addition, rapid deactivation and occurrence of irreversible termination to some extent were governed by persistent radical effect; these contributed to the low concentration of $P_r^\bullet$ during the reaction, which followed pseudo-first order kinetics as shown in Figure 1A.

Effect of Rate Constants on Polymerization Behavior. Debate on the mechanism of Cu(0)-mediated RDRP has received great attention.[24−37,53−55,64,65] The main discrepancies between SET-LRP and SARA ATRP mechanisms are the roles of Cu(0) and Cu^IX/L, which involve the activation of alkyl halides (RX or P_rX) by Cu(0) and Cu^IX/L, as well as the copper-mediated reversible comproportionation disproportionation process. Activation of alkyl halides by "nascent" Cu(0) and the instantaneous disproportionation of Cu^IX/L are supported by SET-LRP mechanism. In SARA ATRP, activation of the alkyl halides is dominated by Cu^IX/L, the disproportionation of Cu^IX/L is limited, and Cu(0) acts as supplemental activator and reducing agent at the same time. Therefore, four key rate constants (i.e., k_{a0}, k_{disp}, k_{a1}, and k_{comp}) involved in the above reactions (Table 1) are discussed below in detail through simulation using the above developed model under the same conditions [Cu(0) wire with l = 4 cm, d = 1 mm, $[MA]_0$:$[MBrP]_0$:$[Me_6TREN]_0$ = 200:1:0.1, V = 4.5 mL, MA/DMSO = 2/1 (v/v), and at 25 °C].

The activation rate constant k_{a0} of Cu(0) influenced the outcome of polymerization as illustrated in Figure 3. For comparison, the black lines ($k_{a0} = 0.2 \times 10^{-4}$ cm·s^{-1}) depicted the same kinetics behavior, as shown in Figure 1. The increase in rate constant from 0.2×10^{-6} to 0.2×10^{-2} cm·s^{-1} implies that the activation rate improved during polymerization, which results in the increasing polymerization rate, as shown in Figure 3A. This result indicates that the initiator (RX) is consumed rapidly and radical concentration ($P^\bullet$) increased dramatically. The higher value of k_{a0} caused deviation from theoretical pseudo-first order kinetics in the semilogarithmic kinetic plot, this plot consisted of two approximately linear domains (orange and blue dashed lines). The nonfirst order kinetic profile also reported by other groups based on experiments and modeling studied on SET-LRP,[26,54] indicate that propagation species in the reaction system should not be constant. In other words, the only cause of deviation in the kinetic plot is the change in radical concentration. Figure 3B shows that all of the evolution of DPn at different simulated k_{a0} deviate from the theoretical DP_n, which is due to insufficient $Cu^{II}X_2/L$ deactivator during the early stage of polymerization. In addition, the slower activation rate significantly increased the time it takes to attain ATRP equilibrium, as illustrated in Figure 3C. At $k_{a0} = 0.2 \times 10^{-6}$ cm·s^{-1}, the evolution of M_w/M_n does not show a "living" characteristic of ATRP even at the end of simulation. Decrease in the development of end functionality in Figure 3D was observed when the activation rate increased. This is attributed to the greater occurrence of irreversible termination that resulted from the higher radical concentration. The simulation results showed that faster activation by Cu(0) leads to deviation in the polymerization kinetic behavior from that in "living" radical polymerization.

dx.doi.org/10.1021/ma501335j | Macromolecules 2014, 47, 6218−6229

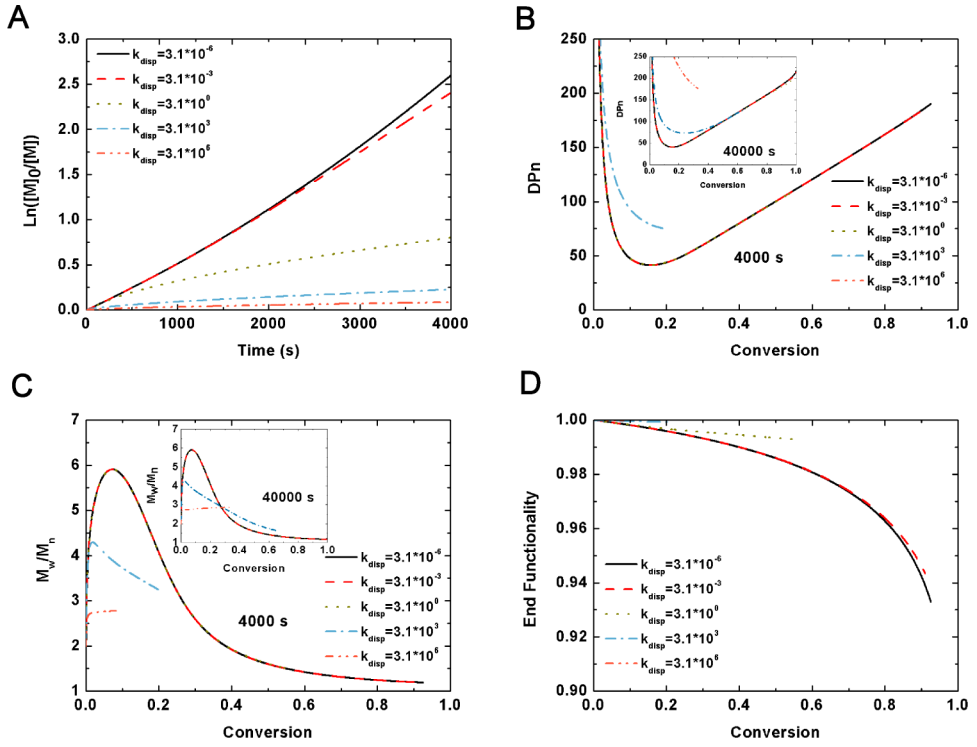

Figure 4. Effect of disproportionation of $Cu^{I}X/L$ (k_{disp}) on kinetics of Cu(0)-mediated RDRP of MA from ref 55: (A) semilogarithmic kinetic plot; (B) evolution of DPn with conversion; (C) evolution of M_w/M_n with conversion; (D) evolution of end functionality with conversion. (Insets represented the simulation results with 40000 s reaction time).

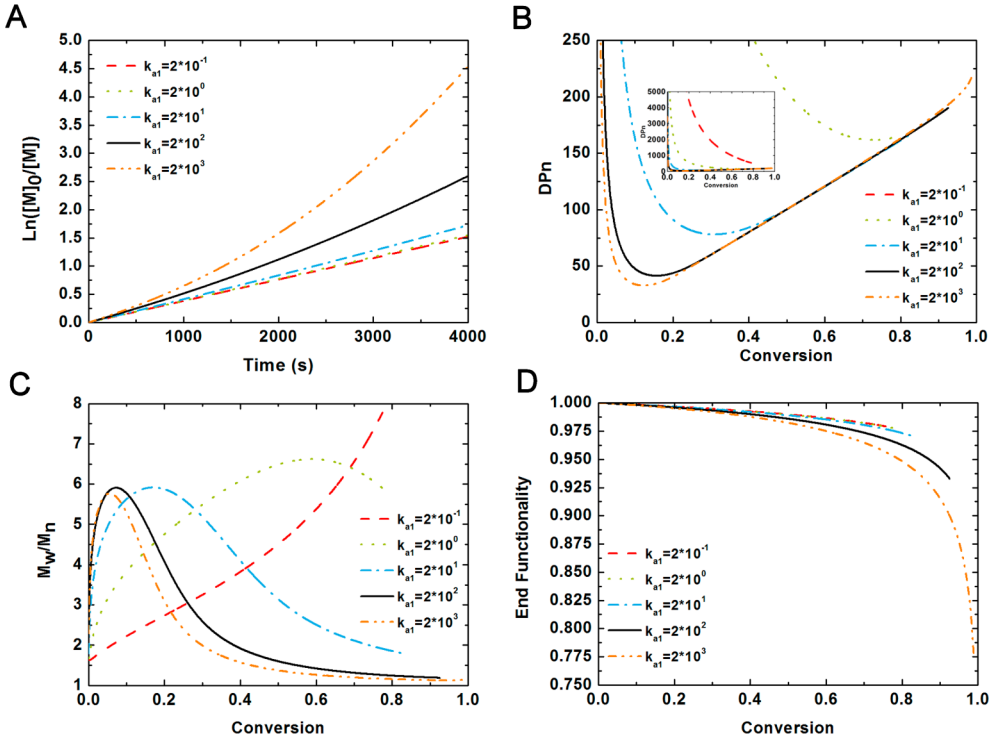

Figure 5. Effect of activation by $Cu^{I}X/L$ (k_{a1}) on kinetics of Cu(0)-mediated RDRP of MA from ref 55: (A) semilogarithmic kinetic plot; (B) evolution of DPn with conversion; (C) evolution of M_w/M_n with conversion; (D) evolution of end functionality with conversion.

The effects of the disproportionation rate constant k_{disp} of $Cu^{I}X/L$ on polymerization kinetics are illustrated in Figure 4. The simulation results (black lines) at $k_{disp} = 3.1 \times 10^{-6}$ cm·s^{-1} exhibited the same kinetics behaviors as those shown in Figure 1. The value of the rate constant changed from 3.1×10^{-6} to 3.1×10^{6} cm·s^{-1} implying that the stability of $Cu^{I}X/L$ significantly declined in polymerization system. Fast disproportionation of $Cu^{I}X/L$ into Cu(0) and $Cu^{II}X_2/L$ claimed in SET-LRP can be taken into account by the value of 3.1×10^{6} cm·s^{-1}. The result shown in Figure 4A demonstrates that the

dx.doi.org/10.1021/ma501335j | Macromolecules 2014, 47, 6218−6229

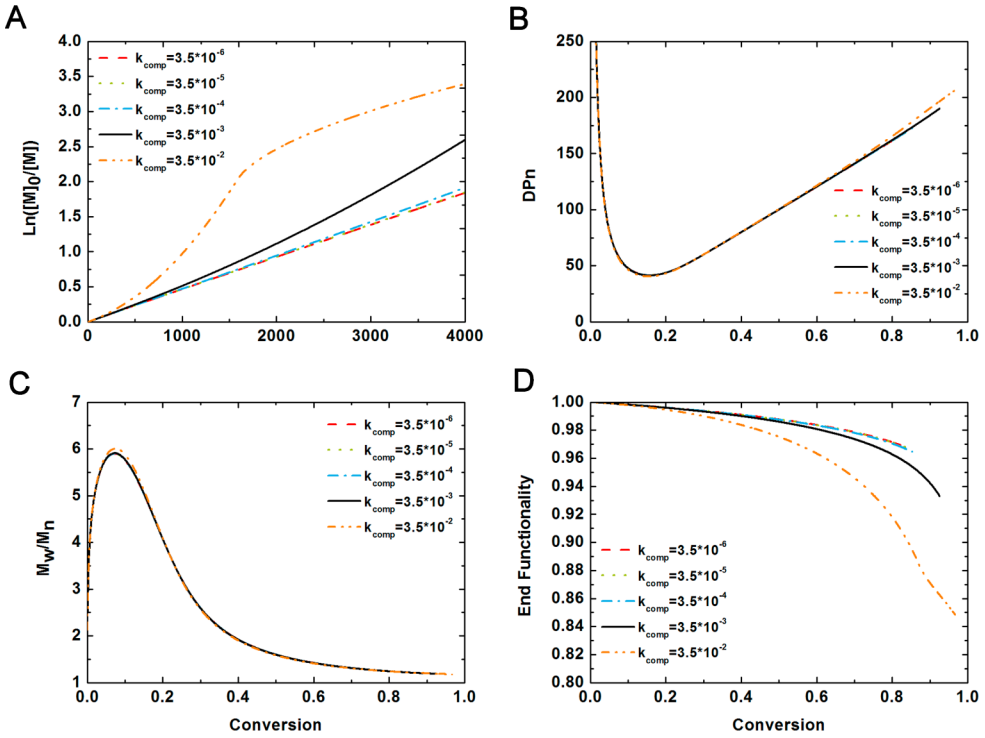

Figure 6. Effect of comproportionation of $Cu^{II}X_2/L$ and Cu(0) (k_{comp}) on kinetics of Cu(0)-mediated RDRP of MA from ref 55: (A) semilogarithmic kinetic plot; (B) evolution of DPn with conversion; (C) evolution of M_w/M_n with conversion; (D) evolution of end functionality with conversion.

increase in disproportionation rate considerably suppressed the ongoing of polymerization. High disproportionation will consume Cu^IX/L rapidly and give an accumulation of $Cu^{II}X_2/L$, which deactivates the radicals generated by the activation by Cu(0) and Cu^IX/L. That is to say, radical concentration is extremely low to make the living radical polymerization run steadily. The offset of DPn still cannot be captured in Figure 4B at about 10% conversion indicates there are only polymer with long chains and relatively high polydispersity (Figure 4C) at $k_{disp} = 3.1 \times 10^6$ cm·s^{-1}. When the simulation with high disproportionation rate was ran up to 40000 s, the conversion of polymerization reaches 40%, but the evolution of DP_n still deviates from theoretical DP_n (Figure 4B inset); additionally, the evolution of M_w/M_n exhibits uncontrollable polymerization feature (atypical trend as shown in Figure 4C inset). A complete description of polymerization kinetics up to 40000 s is shown in Figure S1 in Supporting Information. Figure 4D shows that the end functionality increased with the increase in disproportionation at the same conversion, which stemmed from the lack of irreversible termination at low radical concentration environment. The simulation results illustrate that faster disproportionation of Cu^IX/L do not ensure that the Cu(0)-mediated RDRP of MA proceed successfully during experiment time interval (about 1 h).

Figure 5 shows the assessment results of the different activation rate constants k_{a1} for Cu^IX/L. The value of the rate constant varied from 2×10^{-1} L·mol^{-1}·s^{-1} to 2×10^3 L·mol^{-1}·s^{-1} implying the importance of the role of Cu^IX/L in the alkyl halides activation step of SET-LRP and SARA ATRP. A marked increase in the rate coefficient created a positive impact on the polymerization rate, as shown in Figure 5A. Compared with the outcome of simulation using the value of 2×10^2 L·mol^{-1}·s^{-1} (black lines), the faster activation rate caused higher radical concentration, and thus favored termination. This result led to the evolution of DP_n (>200) that exceeded the theoretical DP_n (DP_n = [MA]/[MBrP] = 200) performed under current experimental conditions in Figure 5B. The first order kinetic plot at slower activation rate shows a promising result for RDRP. However, the zoom-in figure shown in Figure 5B and the evolution of M_w/M_n in Figure 5C show that the polymerization has uncontrollable features. Obviously, the trend in M_w/M_n changed from divergent to convergent as the value of k_{a1} increased. Figure 5D demonstrates the loss of active species in the reaction caused by irreversible termination. The simulation results indicate that slower activation by Cu^IX/L cannot the control molecular weight and its distribution, even when run under first order nature during polymerization.

Insight into the kinetic behavior through variation of the comproportionation rate constant k_{comp} for $Cu^{II}X_2/L$ and Cu(0) is shown in Figure 6. Overall, the effect of k_{comp} on the polymerization outcome is not substantial even with increasing values from 3.5×10^{-6} to 3.5×10^{-2} cm·s^{-1}; this is due to the slow comproportionation in both SET-LRP and SARA ATRP mechanism. However, a faster comproportionation rate (3.1×10^{-2} cm·s^{-1}) can cause polymerization to deviate from first order kinetics having two approximately linear domains (orange dashed lines in Figure 6A). Therefore, the active species concentration in the mixture is not constant and is maintained at relatively high levels. Evolutions of DP_n (Figure 6B) and M_w/M_n (Figure 6C) for different k_{comp} overlapped; difference between the two evolutions were not distinguishable within the simulation interval. Excess of DP_n (>200) and loss of end functionality (Figure 6D) at faster comproportionation rate are explained by the reasons cited above. As a whole, the modeling results demonstrate that comproportionation of $Cu^{II}X_2/L$ and Cu(0) does not predominantly affect the kinetic behavior of

dx.doi.org/10.1021/ma501335j | Macromolecules 2014, 47, 6218−6229

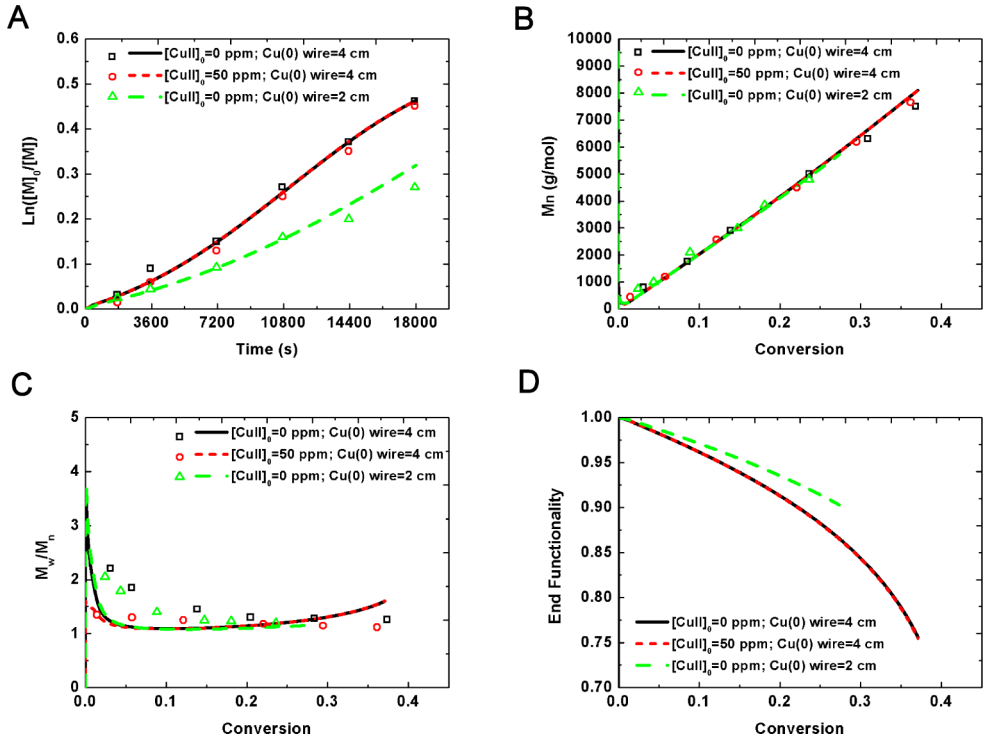

Figure 7. Modeling (lines) and experimental study (symbols) for the kinetics of Cu(0)-mediated RDRP of MMA: (A) semilogarithmic kinetic plot; (B) evolution of DP_n with conversion; (C) evolution of M_w/M_n with conversion; (D) evolution of end functionality with conversion (black line and square data for entry 1; green dashed line and trilateral data for entry 2; red short-dashed line and circle data for entry 3).

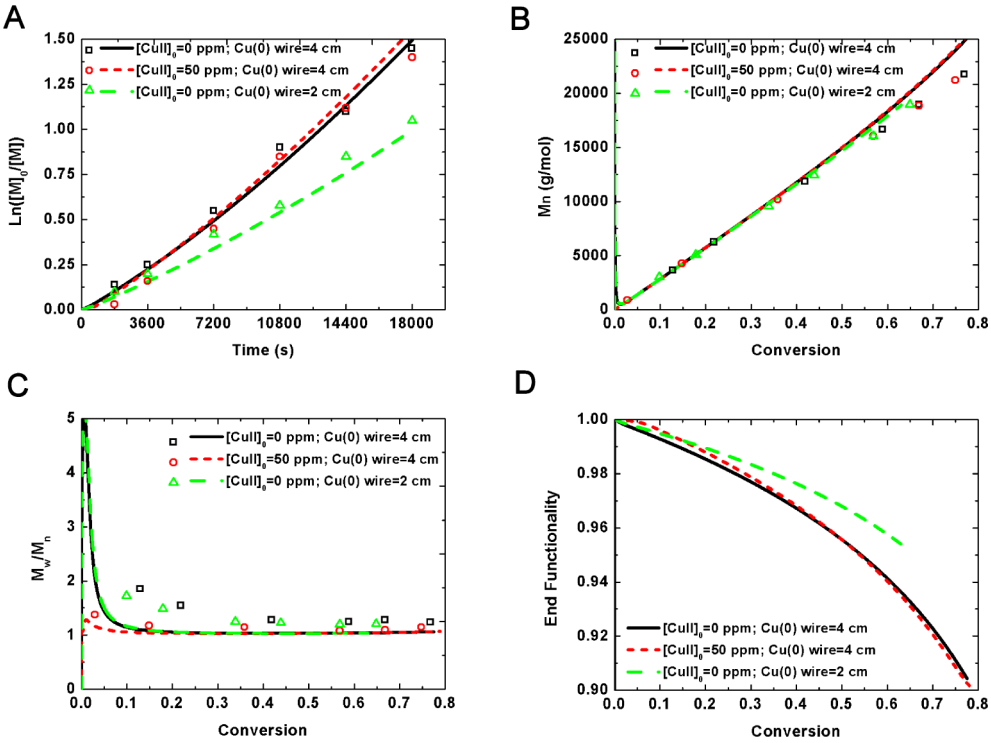

Figure 8. Modeling (lines) and experimental study (symbols) for the kinetics of Cu(0)-mediated RDRP of BMA: (A) semilogarithmic kinetic plot; (B) evolution of DPn with conversion; (C) evolution of M_w/M_n with conversion; (D) evolution of end functionality with conversion (black line and square data for entry 4; green dashed line and trilateral data for entry 5; red short-dashed line and circle data for entry 6).

Cu(0)-mediated RDRP, and an appropriate rate constant can control over the molecular weight and its distribution.

Polymerization of MMA. Detailed studies of Cu(0)-mediated RDRP focus on acrylates because of their high reactivity even at ambient temperature.[24−32] Typically, the polymerization time for an MA system with over 80% conversion is <1 h. However, Cu(0)-mediated RDRP of MMA is far slower than that of MA under identical conditions

dx.doi.org/10.1021/ma501335j | Macromolecules 2014, 47, 6218−6229

because of the lower reactivity of methacrylates. In view of few researches conducted on methacrylate polymerization in the presence of Cu(0),[66−68] the current study selected MMA and BMA system to investigate the kinetic behavior at different conditions (Table 4) by experiments and simulation. The material properties and kinetic constants for simulation are listed in Table 3. It should be pointed out that the kinetic parameters (k_{disp} and k_{comp}) in MMA and BMA cases are assumed to be the same with those in the MA case. This assumption is based on the minor influence of the solvent, monomer, and polymer on Cu(0)-mediated reversible comproportionation-disproportionation process.[31,32] However, the kinetic parameters (k_{a0}, k_{d0}, k_{a1}, k_{d1})for the steps involving the activation and deactivation of alkyl halides (RX or P$_r$X) by Cu(0), Cu(I), and adjustable parameter (B_t) affected by activation/deactivation parameters are optimized in this work on the basis of experiments.

Figure 7 shows the results of the polymerization of MMA at three different conditions. The kinetic plots in Figure 7A appeared to follow approximate first order kinetics in all conditions, which indicate the well controllability and "living" feature of polymerization. The chain-length dependency of the termination reactions considered in simulation is the reason for the slight acceleration phenomenon with ongoing polymerization. In Cu(0)-mediated RDRP, reaction rate should be dependent on the surface area of Cu(0). The kinetic plot (green dashed line and trilateral data) for entry 2 (2 cm Cu(0) wire) shows a lower reaction rate compared with entry 1 (black line and square data, 4 cm Cu(0) wire). According to eq 10, the apparent values (k_p^{app}) for surface areas 1.27 cm^2 and 0.644 cm^2 are $k_{p1}^{app} = 2.57 \times 10^{-5} s^{-1}$ and $k_{p2}^{app} = 1.77 \times 10^{-5} s^{-1}$, respectively. The results are in accordance with the dependence of reaction rate with the square root of the surface area ($k_{p1}^{app}/k_{p2}^{app} \propto (S_1/S_2)^{1/2}$), as reported previously.[32,36,69] Evidently, the lower polymerization rate with lower radical concentration will lead to lower conversion (Figure 7B), but higher end functionality (Figure 7D). In addition, the evolutions of M_n and M_w/M_n for both polymerizations were similar, coupled with large initial M_n and M_w/M_n (Figures 7B and 7C). A shorter transitional period for the attainment of ATRP equilibrium was observed as compared with that in MA polymerization.

In the above discussion (Figure 1), low concentration of deactivator ($Cu^{II}X_2$/L) during the early stage of the reaction can cause the uncontrollable characteristic. From the results of entry 3 (red short-dashed line and circle data, 50 ppm of $Cu^{II}Br_2$) in Figure 7, it can be seen that the reaction rate is almost the same with entry 1, which indicates that the small amount of added deactivator does not affect the apparent polymerization rate (k_p^{app}) as has been confirmed by experiments.[70] Thus, the loss of active species during the reaction should be similar for both systems. However, the extra deactivator has a positive effect on shortening the time needed to attain ATRP equilibrium and controllability. It is presented as theoretically developmental M_n and low M_w/M_n at the start of polymerization macroscopically.

Polymerization of BMA. The kinetic study was also carried out using BMA under three conditions. As shown in Figure 8A, all semilogarithmic kinetic plots followed linear pseudo-first order kinetics. Similarly, the apparent values decreased based on the square root of the surface area from $k_{p4}^{app} = 8.30 \times 10^{-5} s^{-1}$ to $k_{p5}^{app} = 5.53 \times 10^{-5} s^{-1}$ for entries 4 and 5, respectively. When 50 ppm of $Cu^{II}Br_2$ was initially added, a short induction period was observed because of the reduction of Cu^{II} by Cu(0). In parts B and C of Figure 8, there were no significant differences in the evolutions of M_n and M_w/M_n for the polymerizations using different lengths of Cu(0) wire. But, formation of long polymer chains and high polydipersity from start to the end of reaction with addition of $Cu^{II}Br_2$ were not observed (entry 6). Significant improvements were illustrated by simulation and experiment. Figure 8D shows the similar trend of end functionality for the three BMA and MMA systems. But, BMA systems have lesser loss of activator species during the reaction that resulted from the low intrinsic termination rate.

CONCLUSION

A novel and comprehensive kinetic model was developed based on the mechanism of SARA ATRP and was validated by experimental data obtained from a previous study. Simulation results showed that diffusional limitations on termination have significant effects on polymerization. Good agreement between the simulation results and experimental data demonstrated the reliability of the developed model. Concentrations of reactants and rates of reactions during Cu(0)-mediated RDRP were described by simulation, which contributed to the better understanding of the evolution of the species in mixtures that are difficult to measure by experiment.

Effect of major kinetic parameters (i.e., k_{a0}, k_{disp}, k_{a1}, k_{comp}) on kinetic behaviors was also investigated in detail. Simulation results showed that faster activation by Cu(0) leads to the polymerization kinetic behavior deviation from that in living radical polymerization; faster disproportionation of Cu^IX/L cannot ensure the Cu(0)-mediated RDRP of MA to proceed successfully during the experiment time interval (about 1 h); slower activation by Cu^IX/L cannot control the molecular weight and its distribution, even when run under first order nature during polymerization; the comproportionation of $Cu^{II}X_2$/L and Cu(0) does not predominantly affect the kinetic behavior of Cu(0)-mediated RDRP, and an appropriate rate coefficient can control over the molecular weight and its distribution.

Finally, Cu(0)-mediated RDRP of MMA and BMA were performed to study the polymerization kinetics at 25 °C. For both polymerization systems, longer polymerization time was needed due to the lower reactivity of methacrylates. The results of simulations and experiments under polymerization conditions show that the Cu(0) surface area-dependent apparent value follows the relationship of $k_{p1(4)}^{app}/k_{p2(5)}^{app} \propto (S_{1(4)}/S_{2(5)})^{1/2}$ as reported previously. When the initial $Cu^{II}Br_2$ deactivator was added, the controllability of polymerization was dramatically improved as demonstrated by theoretically developmental Mn and low M_w/M_n at the start of polymerization.

Overall, the current study shed light on the underlying mechanism involved in Cu(0)-mediated RDRP by simulation, and optimization of the product quality by experiments was achieved.

ASSOCIATED CONTENT

Supporting Information

The definitions of moments, a set of moment equations, and equations for reaction rates, and a figure showing the effect of disproportionation. This material is available free of charge via the Internet at http://pubs.acs.org.

AUTHOR INFORMATION

Corresponding Author

*(Z.-H.L.) E-mail: luozh@sjtu.edu.cn. Telephone: +86-21-54745602. Fax: +86-21-54745602.

Notes

The authors declare no competing financial interests.

ACKNOWLEDGMENTS

The authors thank the National Natural Science Foundation of China (No. 21276213), the Research Fund for the Doctoral Program of Higher Education (No. 20130073110077) and the National High Technology Research and Development Program of China (No. 2013AA032302) for supporting this work. The authors would like to thank Dr. Fanyou Yan (Key Laboratory for Green Chemical Technology of the State Education Ministry, School of Chemical Engineering and Technology, Tianjin University, China) for his kind suggestions and meaningful contribution to the manuscript.

REFERENCES

(1) Braunecker, W. A.; Matyjaszewski, K. *Prog. Polym. Sci.* **2007**, *32*, 93−146.
(2) Jenkins, A. D.; Jones, R. G.; Moad, G. *Pure Appl. Chem.* **2010**, *82*, 483−491.
(3) Wang, J.-S.; Matyjaszewski, K. *J. Am. Chem. Soc.* **1995**, *117*, 5614−5615.
(4) Kato, M.; Kamigaito, M.; Sawamoto, M.; Higashimura, T. *Macromolecules* **1995**, *28*, 1721−1723.
(5) Matyjaszewski, K.; Tsarevsky, N. V. *Nat. Chem.* **2009**, *1*, 276−288.
(6) Matyjaszewski, K. *Macromolecules* **2012**, *45*, 4015−4039.
(7) Siegwart, D. J.; Oh, J. K.; Matyjaszewski, K. *Prog. Polym. Sci.* **2012**, *37*, 18−37.
(8) Matyjaszewski, K.; Tsarevsky, N. V. *J. Am. Chem. Soc.* **2014**, *136*, 6513−6533.
(9) Fischer, H. *Chem. Rev.* **2001**, *101*, 3581−3610.
(10) Destarac, M. *Macromol. React. Eng.* **2010**, *4*, 165−179.
(11) Chan, N.; Cunningham, M. F.; Hutchinson, R. A. *Macromol. React. Eng.* **2010**, *4*, 369−380.
(12) Chan, N.; Cunningham, M. F.; Hutchinson, R. A. *J. Polym. Sci. A Polym. Chem.* **2013**, *51*, 3081−3096.
(13) Matyjaszewski, K.; Jakubowski, W.; Min, K.; Tang, W.; Huang, J.; Braunecker, W. A.; Tsarevsky, N. V. *Proc. Natl. Acad. Sci. U. S. A.* **2006**, *103*, 15309−15314.
(14) Jakubowski, W.; Matyjaszewski, K. *Angew. Chem., Int. Ed.* **2006**, *45*, 4482−4486.
(15) Magenau, A. J. D.; Strandwitz, N. C.; Gennaro, A.; Matyjaszewski, K. *Science* **2011**, *332*, 81−84.
(16) Konkolewicz, D.; Schröder, K.; Buback, J.; Bernhard, S.; Matyjaszewski, K. *ACS Macro Lett.* **2012**, *1*, 1219−1223.
(17) Visnevskij, C.; Makuska, R. *Macromolecules* **2013**, *46*, 4764−4771.
(18) Zhou, Y. N.; Luo, Z. H. *Polym. Chem.* **2013**, *4*, 76−84.
(19) Zhou, Y. N.; Zhang, Q.; Luo, Z. H. *Langmuir* **2014**, *30*, 1489−1499.
(20) Zhang, Q.; Wilson, P.; Li, Z.; McHale, R.; Godfrey, J.; Anastasaki, A.; Waldron, C.; Haddleton, D. M. *J. Am. Chem. Soc.* **2013**, *135*, 7355−7363.
(21) Chan, N.; Cunningham, M. F.; Hutchinson, R. A. *Polym. Chem.* **2012**, *3*, 486−497.
(22) Hornby, B. D.; West, A. G.; Tom, J. C.; Waterson, C.; Harrisson, S.; Perrier, S. *Macromol. Rapid Commun.* **2010**, *31*, 1276−1280.
(23) Tom, J.; Hornby, B.; West, A.; Harrisson, S.; Perrier, S. *Polym. Chem.* **2010**, *1*, 420−422.
(24) Percec, V.; Guliashvili, T.; Ladislaw, J. S.; Wistrand, A.; Stjerndahl, A.; Sienkowska, M. J.; Monteiro, M. J.; Sahoo, S. *J. Am. Chem. Soc.* **2006**, *128*, 14156−14165.
(25) Rosen, B. M.; Percec, V. *Chem. Rev.* **2009**, *109*, 5069−5119.
(26) Nguyen, N. H.; Levere, M. E.; Kulis, J.; Monteiro, M. J.; Percec, V. *Macromolecules* **2012**, *45*, 4606−4622.
(27) Levere, M. E.; Nguyen, N. H.; Percec, V. *Macromolecules* **2012**, *45*, 8267−8274.
(28) Zhang, N.; Samanta, S. R.; Rosen, B. M.; Percec, V. *Chem. Rev.* **2014**, *114*, 5848−5958.
(29) Matyjaszewski, K.; Tsarevsky, N. V.; Braunecker, W. A.; Dong, H.; Huang, J.; Jakubowski, W.; Kwak, Y.; Nicolay, R.; Tang, W.; Yoon, J. A. *Macromolecules* **2007**, *40*, 7795−7806.
(30) Zhang, Y. Z.; Wang, Y.; Peng, C. H.; Zhong, M. J.; Zhu, W. P.; Konkolewicz, D.; Matyjaszewski, K. *Macromolecules* **2012**, *45*, 78−86.
(31) Wang, Y.; Zhong, M.; Zhu, W.; Peng, C.-H.; Zhang, Y.; Konkolewicz, D.; Bortolamei, N.; Isse, A. A.; Gennaro, A.; Matyjaszewski, K. *Macromolecules* **2013**, *46*, 3793−3802.
(32) Peng, C.-H.; Zhong, M.; Wang, Y.; Kwak, Y.; Zhang, Y.; Zhu, W.; Tonge, M.; Buback, J.; Park, S.; Krys, P.; Konkolewicz, D.; Gennaro, A.; Matyjaszewski, K. *Macromolecules* **2013**, *46*, 3803−3815.
(33) Konkolewicz, D.; Wang, Y.; Zhong, M.; Krys, P.; Isse, A. A.; Gennaro, A.; Matyjaszewski, K. *Macromolecules* **2013**, *46*, 8749−8772.
(34) Konkolewicz, D.; Krys, P.; Góis, J. R.; Mendonça, P. V.; Zhong, M.; Wang, Y.; Gennaro, A.; Isse, A. A.; Fantin, M.; Matyjaszewski, K. *Macromolecules* **2014**, *47*, 560−570.
(35) West, A. G.; Hornby, B.; Tom, J.; Ladmiral, V.; Harrisson, S.; Perrier, S. *Macromolecules* **2011**, *44*, 8034−8041.
(36) Harrisson, S.; Couvreur, P.; Nicolas, J. *Macromolecules* **2012**, *45*, 7388−7396.
(37) Harrisson, S.; Nicolas, J. *ACS Macro Lett.* **2014**, *3*, 643−647.
(38) Zhu, S. P. *Macromol. Theory Simul.* **1999**, *8*, 29−37.
(39) Delgadillo-Velazquez, O.; Vivaldo-Lima, E.; Quintero-Ortega, I. A.; Zhu, S. P. *AIChE J.* **2002**, *48*, 2597−2608.
(40) Wang, R.; Luo, Y. W.; Li, B. G.; Zhu, S. P. *AIChE J.* **2007**, *53*, 174−186.
(41) Tang, W.; Matyjaszewski, K. *Macromol. Theory Simul.* **2008**, *17*, 359−375.
(42) D'Hooge, D. R.; Reyniers, M. F.; Marin, G. B. *Macromol. React. Eng.* **2009**, *3*, 185−209.
(43) D'hooge, D. R.; Reyniers, M.-F.; Stadler, F. J.; Dervaux, B.; Bailly, C.; Du Prez, F. E.; Marin, G. B. *Macromolecules* **2010**, *43*, 8766−8781.
(44) D'hooge, D. R.; Konkolewicz, D.; Reyniers, M.-F.; Marin, G. B.; Matyjaszewski, K. *Macromol. Theory Simul.* **2012**, *21*, 52−69.
(45) Al-Harthi, M.; Masihullah, J. K.; Abbasi, S. H.; Soares, J. B. P. *Macromol. Theory Simul.* **2009**, *18*, 307−316.
(46) Al-Harthi, M.; Khan, M. J.; Abbasi, S. H.; Soares, J. B. P. *Macromol. React. Eng.* **2009**, *3*, 148−159.
(47) Zhou, Y. N.; Li, J. J.; Luo, Z. H. *J. Polym. Sci., Part A: Polym. Chem.* **2012**, *50*, 3052−3066.
(48) Zhou, Y. N.; Luo, Z. H.; Chen, J. H. *AIChE J.* **2013**, *59*, 3019−3033.
(49) Li, J. J.; Luo, Z. H. *Ind. Eng. Chem. Res.* **2014**, *53*, 1900−1908.
(50) Zhou, Y.-N.; Luo, Z.-H. *J. Polym. Sci., Part A: Polym. Chem.* **2014**, *52*, 2228−2238.
(51) Li, X.; Wang, W. J.; Li, B. G.; Zhu, S. P. *Macromol. React. Eng.* **2011**, *5*, 467−478.
(52) Payne, K. A.; D'Hooge, D. R.; Van Steenberge, P. H. M.; Reyniers, M. F.; Cunningham, M. F.; Hutchinson, R. A.; Marin, G. B. *Macromolecules* **2013**, *46*, 3828−3840.
(53) Monteiro, M. J.; Guliashvili, T.; Percec, V. *J. Polym. Sci., Part A: Polym. Chem.* **2007**, *45*, 1835−1847.
(54) Haehnel, A. P.; Fleischmann, S.; Hesse, P.; Hungenberg, K.-D.; Barner-Kowollik, C. *Macromol. React. Eng.* **2013**, *7*, 8−23.
(55) Zhong, M.; Wang, Y.; Krys, P.; Konkolewicz, D.; Matyjaszewski, K. *Macromolecules* **2013**, *46*, 3816−3827.
(56) Ahmad, N. M.; Charleux, B.; Farcet, C.; Ferguson, C. J.; Gaynor, S. G.; Hawkett, B. S.; Heatley, F.; Klumperman, B.; Konkolewicz, D.;

Lovell, P. A.; Matyjaszewski, K.; Venkatesh, R. *Macromol. Rapid Commun.* **2009**, *30*, 2002−2021.
(57) Fedors, R. F. *J. Polym. Sci., Polym. Lett. Ed.* **1979**, *17*, 719−722.
(58) Berthet, R.; Chalamet, Y.; Taha, M.; Zerroukhi, A. *Macromol. Mater. Eng.* **2006**, *291*, 720−731.
(59) Wisniak, J.; Cortez, G.; Peralta, R. D.; Infante, R.; Elizalde, L. E.; Amaro, T. A.; García, O.; Soto, H. *J. Chem. Thermodyn.* **2008**, *40*, 1671−1683.
(60) Beuermann, S.; Buback, M.; Davis, T. P.; Gilbert, R. G.; Hutchinson, R. A.; Kajiwara, A.; Klumperman, B.; Russell, G. T. *Macromol. Chem. Phys.* **2000**, *201*, 1355−1364.
(61) Buback, M.; Junkers, T. *Macromol. Chem. Phys.* **2006**, *207*, 1640−1650.
(62) Beuermann, S.; Buback, M.; Davis, T. P.; Gilbert, R. G.; Hutchinson, R. A.; Olaj, O. F.; Russell, J.; Schweer, G. T.; Van Herk, A. M. *Macromol. Chem. Phys.* **1997**, *198*, 1545−1560.
(63) Goto, A.; Fukuda, T. *Prog. Polym. Sci.* **2004**, *29*, 329−385.
(64) Isse, A. A.; Gennaro, A.; Lin, C. Y.; Hodgson, J. L.; Coote, M. L.; Guliashvili, T. *J. Am. Chem. Soc.* **2011**, *133*, 6254−6264.
(65) Guliashvili, T.; Mendonça, P. V.; Serra, A. C.; Popov, A. V.; Coelho, J. F. J. *Chem.—Eur. J.* **2012**, *18*, 4607−4612.
(66) Percec, V.; Guliashvili, T.; Popov, A. V.; Ramirez-Castillo, E.; Hinojosa-Falcon, L. A. *J. Polym. Sci., Part A: Polym. Chem.* **2005**, *43*, 1660−1669.
(67) Zhang, Z.; Wang, W.; Xia, H.; Zhu, J.; Zhang, W.; Zhu, X. *Macromolecules* **2009**, *42*, 7360−7366.
(68) Fleischmann, S.; Percec, V. *J. Polym. Sci., Part A: Polym. Chem.* **2010**, *48*, 2243−2250.
(69) Nguyen, N. H.; Rosen, B. M.; Lligadas, G.; Percec, V. *Macromolecules* **2009**, *42*, 2379−2386.
(70) Nguyen, N. H.; Rosen, B. M.; Percec, V. *J. Polym. Sci., Part A: Polym. Chem.* **2010**, *48*, 1752−1763.